Journal of
Mechanical
Science and
Technology

Journal of Mechanical Science and Technology 21 (2007) 1263~1270

Thermo-Hydraulic Characteristics of Hybrid Mixing Vanes in a 17x17 Nuclear Rod Bundle

Cheol-Min Lee[b,*], Jeong-Soo An[b], Young-Don Choi[a]

[a]*Professor, Department of Mechanical Engineering, Korea University, Anamdong, Sungbukku, Seoul 136-701, Korea*
[b]*Department of Mechanical Engineering, Graduate School, Korea University, Anamdong, Sungbukku, Seoul 136-701, Korea*

(Manuscript Received September 18, 2006; Revised May 2, 2007; Accepted May 15, 2007)

Abstract

The lateral flow in the sub-channel of a nuclear rod bundle increase turbulent mixing and enhance heat transfer rate and safety. Various types of mixing vanes have been investigated to produce more lateral flow. In this study, the thermal-hydraulic characteristics of Hybrid mixing vane in a 17x17 rod bundle were calculated. Hybrid mixing vane has bended root part and split stem part. The computation was performed using a supercomputer due to the high number of grid meshes. The characteristics of Hybrid mixing vane were compared to Split mixing vane. The Hybrid mixing vane showed higher values of secondary intensity, cross-sectional turbulence intensity and Nu number and lower values of maximum temperature and standard deviation of temperature. Meanwhile, The Hybrid mixing vane has higher invariance because small vortexes travel, stretch and are connected with main stream.

Keywords: Split mixing vane; Hybrid mixing vane; Nuclear fuel rod bundle; Subchannel

1. Introduction

Spacer grids in the nuclear fuel rod assembly maintain a constant distance between the rods and secure a coolant flow passage. Mixing vanes, usually attached to the spacer grids, induce vortex flows in the sub-channels that generate turbulence and promote thermal mixing between subchannels. This helps to enhance the heat transfer performance of the sub-channels in a nuclear reactor.

Mixing vanes spread the heat from the fuel rods to the coolant. If the heat generated from the fuel rods cannot be dissipated well into the coolant, heat is concentrated locally and heat transfer rate is decreased.

The design of the mixing vane shape for the fuel assembly was optimized through both computation (In et al., 2001) and experimentation (Ibragimov et al., 1965).

Computational analysis of full scale rod bundle has been difficult for insufficient computer resources. So the flow patterns of reduced rod bundle have been main studies just like a single sub-channel (In et al., 2001 and Wang et al., 2001), hexagonal 7rod bundle (Haldar, 2000), rectangular 16 rod bundle (Shen et al., 1991 and Yue et al., 1991), hexagonal 19 rod bundle (Rehme and Trippe, 1979) and rectangular 25 and 36 rod bundles (Yang and Chung, 1995).

In this paper, the full range of rectangular 289 rod bundle with 8 sets of mixing vanes is calculated using the IBM 690 supercomputer with a parallel system.

The most prevalent mixing vane is Split type and that makes a small scale vortex flow. Figure 1(a) shows the schematic shape of a Split mixing vane. Split mixing vanes create a vortex flow confined to

*Corresponding author. Tel.: +82 2 926 5908, Fax.: +82 2 926 9290
E-mail address: jngyl00@korea.ac.kr

each subchannel so they generate little cross-flow between the subchannels. Furthermore, the turbulence caused by the Split mixing vanes decays rapidly due to its small scale.

On the other hand, bend type mixing vane makes a large scale vortex flow. So it is named as LSVF mixing vane and the shape is shown in Fig. 1(b). LSVF mixing vanes can maintain turbulence intensity for longer periods than Split mixing vanes (Park, 2001). But, LSVF mixing vanes have greater pressure losses and a higher rod surface temperature than Split type (Lee and Choi, 2005).

In this study, the Hybrid type mixing vane is suggested. Figure 1(c) shows the shape of a Hybrid mixing vane. The Hybrid mixing vane has the bended root part and the split stem part.

The thermo-hydraulic characteristics of Hybrid mixing vanes are compared with those of Split mixing vanes. To guarantee a fair comparison, the same blocking ratio of 0.39 is applied. The blocking ratio is the value of the blocking area of a mixing vane divided by the sub-channel area.

The coolant mixing is composed of conduction and convection, and convection is much greater than conduction. Convection is mainly affected with secondary flow and cross-sectional turbulence intensity. So, secondary flow and cross-sectional turbulence intensity are analyzed in this study.

(a) Split mixing vane

(b) LSVF mixing vane

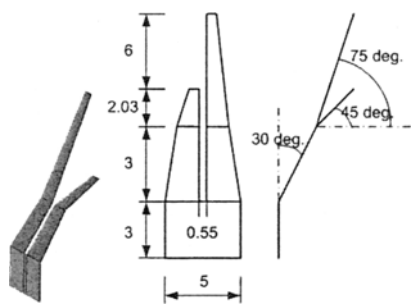

(c) Hybrid mixing vane

Fig. 1. Schematic shapes of mixing vane.

2. Computational method

2.1 Computational geometry

In this study, a 17x17 square type rod bundle with 8 spans of spacer grids is adopted for the computational model. A "span" means the length between two spacer grids. The bundle has 289 rods in total, including 264 heating rods, 24 control rods and 1 supporting rod. Mixing vane is attached at the end of spacer grid. Spacer grid system is installed in every $33D_h$ in the axial direction.

Figure 2 shows the computational geometry and the specifications of the rod bundle are listed in Table 1.

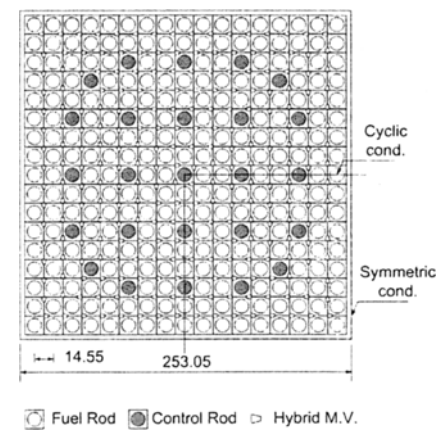

(a) Cross-sectional shape

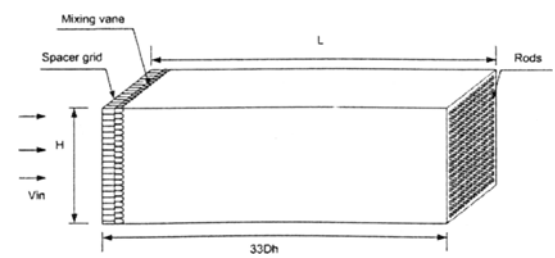

(b) Longitudinal shape (1 span)

Fig. 2. Computational geometry. (total 8 spans)

Table 1. Rod bundle channel data.

Parameter	Unit	Dimension
Rod Diameter	mm	10.6
Rod Pitch	mm	14.55
Spacer Grid Pitch	mm	522
Housing	mm	253.05
Hydraulic Diameter	mm	16.0
Vane Bending Angle	degree	30
Heating Rods	piece	264
Non-heating Rod	piece	25

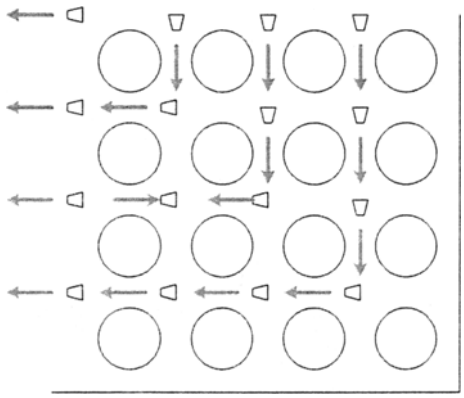

(a) Hybrid-parallel

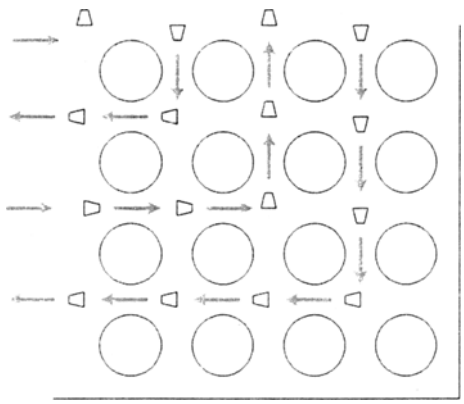

(b) Hybrid-counter

Fig. 3. Arraying methods of Hybrid type mixing vanes.

Figure 3 shows the arraying methods of Hybrid mixing vane. In Hybrid-parallel method, all the mixing vanes are counter-clock-wise direction. And in Hybrid-counter method, the mixing vanes are clock-wise direction and counter-clockwise direction alternatively.

The grid system is shown in Fig. 4. A quarter of the rod bundle is computed using a cyclic boundary condition. About 13.2 million structured volume

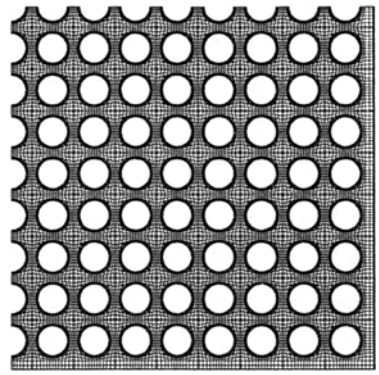

(a) Cross-sectional meshes

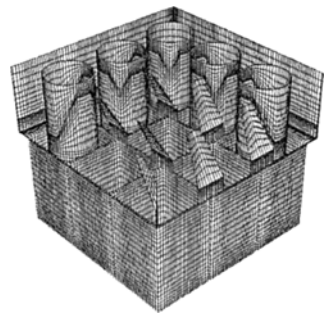

(b) Part of mesh structure

Fig. 4. Mesh structure.

meshes are generated. The mesh is concentrated near the rod, spacer grid and mixing vane where the velocity gradient is high.

Mesh density can affect computational results. If higher mesh density produce different flow pattern, grid system should be revised. The present grid mesh number is 13.2million. Additional two case of grid system for 16.3 million and 8.17 million meshes are tested. Rod bundle with spacer grid with no mixing vanes is adopted as test geometry.

The secondary flow intensity, VI_{cross}, is defined as the surface average of lateral velocity divided by the axial bulk velocity as described in Eq. (1).

$$VI_{cross} = \frac{1}{A}\int\left(\frac{\sqrt{U_1^2+U_2^2}}{U_{3,bulk}}\right)dA \tag{1}$$

Secondary flow intensity for the three kinds of meshes are shown in Fig. 5. Secondary flow intensities are increased after spacer grid and drop. They show the same patterns regardless of the mesh numbers.

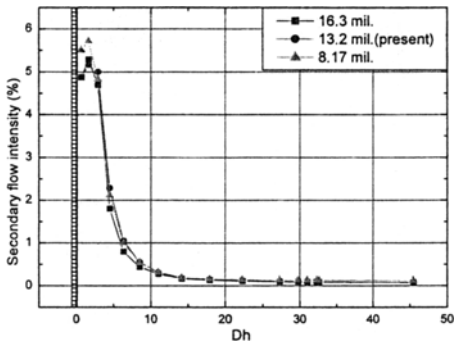

Fig. 5. Grid tests of secondary flow intensities.

Pressure and turbulent intensity also show the same patterns the higher meshed case, and the grid system is verified as reliable.

2.2 Computational condition

Table 2 shows the list of boundary conditions.

The inlet temperature is 564.817 K and inlet pressure is 10 MPa. The working fluid has a 29% lower density, a 27% higher specific heat and a 91% lower viscosity than the natural state (25 degree centigrade and 1bar) of the liquid water. And it result in about 10 times higher Reynolds number.

The quarter cut face has the cyclic condition and the housing face has the symmetry condition.

To manage the 13.2 million meshes, the IBM supercomputer in KISTI (Korea Institute of Science and Technology Information) is used. The ftp and X-window programs are used for the data transfer and operation. And the Kon shell is used for the UNIX program.

Usually, k-epsilon model and RSM (Reynolds Stress Equations Model) model are used to analyze turbulence. The k-epsilon model is used for simple isotropic turbulence and RSM model for anisotropic turbulence. To analyze lateral element of turbulence and vortex structure of rod bundle, we adopted RSM model for turbulence model. And before usage of RSM, the convergence of the k-ε model is preceded to avoid divergence. Iterations using RSM continued until the residual is under 1e-4 and steady. And the FLUENT code is used for calculation.

Table 2. Boundary conditions.

Boundary	Unit	Value
Inlet Velocity	m/s	4.326
Inlet Reynolds Number		542,000
Inlet Temperature	K	564.817
Pressure	Mpa	10
Fuel Rod Heat Flux	kW/m^2	598.7
Housing		Symmetry
Quarter cutting face		Cyclic

2.3 Computational method

The equations used in calculation are explained below (FLUENT Inc., 2001). The rate of increase of mass inside the element is equal to the net rate of the mass flow into the element across its faces.

$$\frac{\partial \rho U_i}{\partial x_i} = 0 \tag{2}$$

Equation (2) is the steady, three-dimensional mass conservation or continuity equation at a point in an incompressible fluid.

Newton's second law states that the rate of change of momentum of a fluid particle equals the sum of the forces on the particle. The balance of momentum is induced as:

$$\frac{\partial U_i U_j}{\partial x_j} = \frac{\partial}{\partial x_i}\left[\nu\left(\frac{\partial U_i}{\partial x_j}+\frac{\partial U_j}{\partial x_i}\right)-\overline{u_i u_j}\right]-\frac{\partial P}{\rho \partial x_i} \tag{3}$$

To obtain the $\rho\overline{u_i u_j}$ in the momentum equation, The exact equation for the transport of Reynolds stress takes the following form:

$$\frac{D\overline{u_i u_j}}{Dt} = P_{ij} + D_{ij} - \varepsilon_{ij} + \phi_{ij} \tag{4}$$

This equation describes six partial differential equations and contains six independent Reynolds stresses ($\overline{u_1^2}$, $\overline{u_2^2}$, $\overline{u_3^2}$, $\overline{u_1 u_2}$, $\overline{u_2 u_3}$ and $\overline{u_1 u_3}$).

CFD computations with the Reynolds stress transport equations retain the production term in its exact form.

$$P_{ij} = -\left(\overline{u_i u_k}\frac{\partial U_j}{\partial x_k}+\overline{u_j u_k}\frac{\partial U_i}{\partial x_k}\right) \tag{5}$$

The diffusion term D_{ij} can be modeled by the assumption that the rate of transport of the Reynolds stresses by diffusion is proportional to the gradient of the Reynolds stresses. The gradient diffusion idea recurs throughout turbulence modeling.

$$D_{ij} = \frac{\partial}{\partial x_k}\left(\frac{\nu_t}{\sigma_k}\frac{\partial \overline{u_i u_j}}{\partial x_k}\right) \quad (6)$$

with $\nu_t = C_\mu \frac{k^2}{\varepsilon}$; $C_\mu = 0.09$ and $\sigma_k = 1.0$

The dissipation rate ε_{ij} is modeled by assuming the small dissipative eddies are isotropic. It is set also that it affects the normal Reynolds stresses (i=j) only and in equal measure. This can be achieved by:

$$\varepsilon_{ij} = \frac{2}{3}\rho\varepsilon\delta_{ij}\left(1+\frac{2k}{\gamma RT}\right) \quad (7)$$

The pressure-strain interaction term ϕ_{ij} constitutes both the most difficult and the most important term to model accurately. Their effects on the Reynolds stresses are caused by two distinct physical processes: pressure fluctuations due to two eddies interacting with each other and pressure fluctuations due to the interaction of an eddy within a region of flow of different mean velocities. The overall effect of the pressure-strain term is to re-distribute energy amongst the normal Reynolds stresses (i=j) so as to make them more isotropic and to reduce the Reynolds shear stresses (i≠j). This can be achieved by:

$$\begin{aligned}\phi_{ij} = &-a_{ij}\left(C_1 + C_1'\frac{P_k}{\varepsilon}\right)\frac{k}{T} + C_2\left(a_{ik}a_{kj} - \frac{1}{3}A_2\delta_{ij}\right)\frac{k}{T} \\ &+\left(C_3 - C_3'\sqrt{A_2}\right)S_{ij}k + C_4\left(a_i S_{kj} + a_{jk}S_{ki} - \frac{2}{3}\delta_{ij}\right)k \\ &+C_5\left(a_{ik}\Omega^A_{kj} + a_{jk}\Omega^A_{ki}\right)k \end{aligned} \quad (8)$$

where Ω^A_{ij} is Coriolis force term, a_{ij} is aniso-tropy vector and A_2 is second invariance. The cons-tants are listed in Fluent Inc.(1991).

The energy equation is derived from the first law of thermodynamics which states that the rate of change of energy of a fluid particle is equal to the rate of heat addition to the fluid particle plus the rate of work done on the particle.

The balance of energy is induced as:

$$\frac{\partial \rho U_i \Theta}{\partial x_j} = \frac{\partial}{\partial x_j}\left(\frac{\mu}{\Pr}\frac{\partial \Theta}{\partial x_j} - \rho\overline{u_i\theta}\right) \quad (9)$$

To obtain the $\rho\overline{u_i\theta}$ in the energy equation, the following turbulence models are employed as Boussinesq's theory:

$$\overline{u_i\theta} = -\frac{\nu_t}{\sigma_\theta}\frac{\partial \Theta}{\partial x_i} \quad (10)$$

3. Numerical results and discussion

The secondary flow intensity, VI_{cross}, means the ratio between lateral velocity and axial velocity.

Figure 6 shows the abrupt increase of VI_{cross} near the spacer grids and mixing vane. Hybrid type mixing vanes show higher VI_{cross} than Split mixing vanes in each span. VI_{cross} generated by Hybrid mixing vanes decays slowly than that of Split mixing vanes.

Euler number, Eu, is non-dimensional parameter indicating pressure difference divided by dynamic pressure as described in Eq. (11).

$$\mathrm{Eu} = \frac{\Delta P}{0.5\rho U^2_{3,bulk}} \quad (11)$$

where ρ is the fluid density and $U_{3,bulk}$ is axial bulk velocity.

Figure 7 shows the variation Euler number in the axial direction for the 3 kinds of mixing vanes.

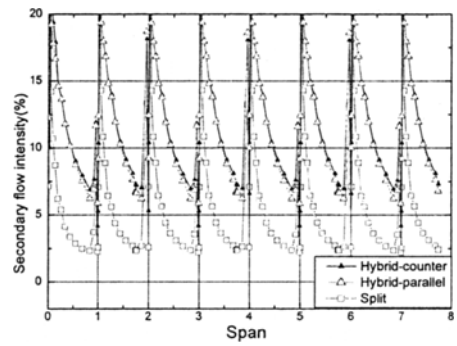

Fig. 6. Axial development of secondary flow intensity.

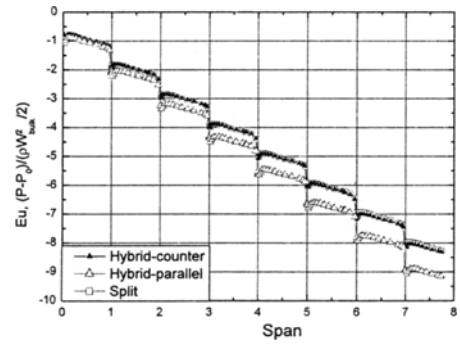

Fig. 7. Axial development of pressure drop.

Spacer grid and mixing vane is located at span 0, 1, 2, 3···. And when the flow passes the mixing vanes, the mixing vanes act as resistance and pressure decreases. Hybrid-counter type shows similar pressure drop with Split type. However, Hybrid-parallel type shows higher pressure drop and require more pump power than Split type. Consequently, Hybrid-counter type shows better characteristics in the field of pressure drop.

Cross-sectional turbulence intensity, TI_{cross}, is composed of the lateral components of turbulence intensity, as described in Eq. (12).

$$TI_{cross} = \frac{1}{A}\int\left(\frac{\sqrt{\overline{u_1^2}+\overline{u_2^2}}}{U_{3,bulk}}\right)dA \tag{12}$$

TI_{cross} is important because it mainly effects to turbulence intensity. Hybrid-counter type has higher value of TI_{cross} than Hybrid-parallel type and Split type has the lowest TI_{cross} as shown in Fig. 8. It means that arraying method effects to turbulence intensity and Hybrid-counter type induce more turbulence mixing.

Each fuel rod releases a constant heat flux so that the mean temperature increases linearly along the main axis regardless of mixing vane type. But maximum temperature differs with the type of mixing vane.

Figure 9 shows maximum temperature distribution, Tmax, with main axis. Hybrid-counter case has lower maximum temperature. It means that the Hybrid-counter type offers better heat transfer rate and safety than the Split type. However Hybrid-parallel type shows the highest maximum temperature and lower safety.

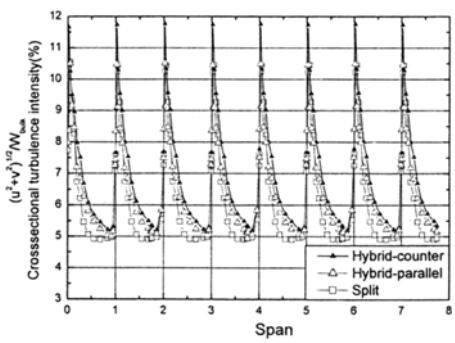

Fig. 8. Axial development of cross-sectional turbulence intensity.

Figure 10 shows the standard deviation of temperature, σ_T, which indicates the thermal non-uniformity. σ_T is defined as Eq. (13).

$$\sigma_T = \sqrt{\frac{1}{A}\int\left(T - T_{avg}\right)^2 dA} \tag{13}$$

Lower value of σ_T means high heat transfer rate. Hybrid-couple type shows the best result and Split type shows the worst result. Meanwhile, Hybrid-parallel type shows good result at earlier span, but shows worse result in downstream.

The Nusselt number is the heat transfer coefficients divided by k/D_h as shown in Eq. (14).

$$Nu = \frac{hD_h}{k} \tag{14}$$

Figure 11 shows ΔNu between Split type which means that Nu of an arbitrary mixing vane minus Nu of SSVF-single mixing vane. Hybrid types show positive value of ΔNu and it means that Hybrid types have higher Nu number than Split type mixing vane.

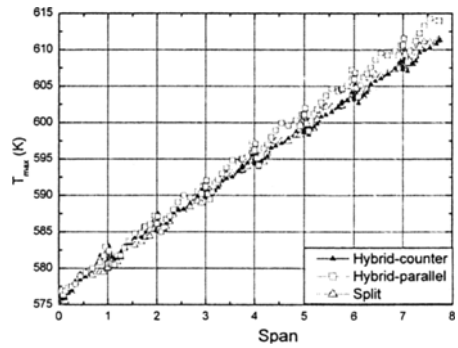

Fig. 9. Axial development of temperature.

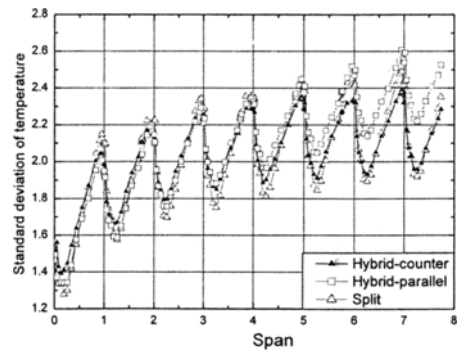

Fig. 10. Axial development of standard deviation of temperature.

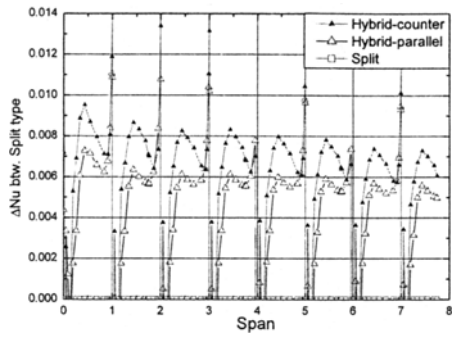

Fig. 11. Axial development of Nu number.

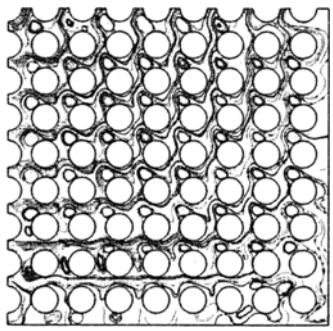

(a) Split

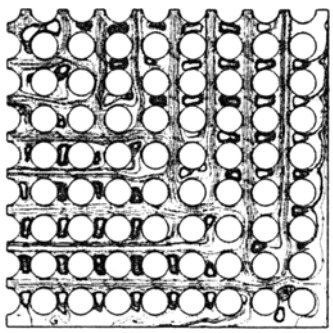

(b) Hybrid-counter

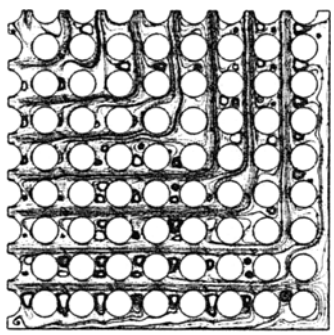

(c) Hybrid-parallel

Fig. 12. Vortexes at 0.15 spans.

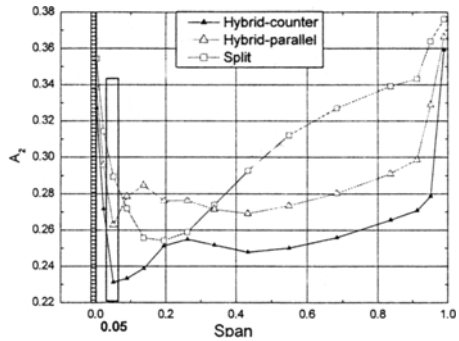

Fig. 13. Axial development of A_2.

Figure 12 shows the vortex structures at 0.15 spans. Vortexes of Split type remain in nearly all subchannels. And more vortexes of Hybrid types are connected earlier than Split type. However, vortexes in a subchannel of Split case hardly travel, stretch and be connected. They have only reduction of size and sphere-like deformation. The vortexes of Split case deforms slowly than those of Hybrid cases.

To investigate anisotropy, Invariance, A_2, is used and can be calculated as Eq. (15).

$$A_2 = a_{ij} a_{ji} \tag{15}$$

with $a_{ij} = \dfrac{\overline{u_i u_j}}{k} - \dfrac{2}{3}\delta_{ij}$

Higher A_2 means higher anisotropy.

A_2 decrease behind the mixing vanes and rebound at 0.2 span for Split type and at 0.05 span for Hybrid types as shown in Fig. 13.

At the location of rebound of A_2, many vortexes are connected. And the connection of vortexes induce higher turbulence mixing. Hybrid cases show earlier connection of vortexes and better turbulence mixing than Split case.

4. Concluding remarks

In this paper, the subchannel flows in the 17x17 rod bundles attached with 3 types of mixing vanes were simulated by an IBM supercomputer.

Hybrid-counter type mixing vanes displayed either better or similar results in secondary flow intensities, pressure drops, cross-sectional turbulent intensity, maximum temperature of the rods, standard deviation of temperature and Nu number than either Split or Hybrid-parallel mixing vanes.

These results imply the importance of mixing vanes and array patterns. Consequently, Hybrid-counter mixing vanes offer better thermo-hydraulic characteristics than Hybrid-parallel and Split mixing vanes.

These results are because that the Hybrid type makes earlier connection of vortexes which are made behind the mixing vane than Split type.

Acknowledgement

This work was supported by Ministry of Commerce, Industry and Energy (Grant No. R-2002-0234).

The authors would like to acknowledge the support from KISTI (Korea Institute of Science and Technology Information) under "The Eighth Strategic Supercomputing Support Program" with Dr. Sangmin Lee as the technical supporter. The use of the computing system of the Supercomputing Center is also greatly appreciated.

References

An, J. S. and Choi, Y. D., 2006, "A Study of Heat Transfer Characteristics of Large Scale Vortex Flow Mixing Vane of Nuclear Fuel Rod Bundle," *Transactions of the KSME B 30*, 24~31.

FLUENT Inc., 2001, Fluent 6.0 user's guide

Haldar, S.C., 2000, "Fully Developed Combined Convection in a Seven-rod Horizontal Bundle," *International Journal of Heat and Mass Transfer 43*, 3735~3742.

Ibragimov, M. K., Isupov, I. V., Kobzar, L. L. and Subbotin, V. I., 1966. "Calculation of the Tangential Stresses at the Wall in a Channel and the Velocity Distribution in a Turbulent Flow of Liquid," *Atomic Energy 21*, 731~739.

In, W. K., Oh, D. S. and Chun, T. H., 2001. "Flow Analysis for Optimum Design of Mixing Vane in a PWR Fuel Assembly," *J. of KNS 33*, 327~338.

Jian, Su, Atila, P. and Silva, Freire, 2002. "Analytical Prediction of Friction Factors and Nusselt Numbers of Turbulent Forced Convection in Rod Bundles with Smooth and Rough Surfaces," *Nucl. Engng. and Design 215*, pp. 111~127.

Lee, C. M. and Choi, Y. D., 2005, "Study on the Optimization of Mixing Vane for LSVF(Large Scale Secondary Vortex Flow) in 17×17 rod bundle," *KSME Autumn Conference*, pp. 373~378.

Lee, K. B., Jang, H. C. and Lee, S. K., 1994. "Study of the Secondary Flow Effect on the Turbulent Flow Characteristics in Fuel Rod Bundles," *J. of KNS 26*, 345~354.

Lee, S. Y. and Choi, Y. D., 2003. "Turbulence Generation by Ultrasonically Induced Gaseous Cavitation in the CO_2 Saturated Water Flow," *KSME International Journal 17*, 1203~1210.

Park, J. S., 2001. "A Study of Turbulent Heat Transfer Performance Enhancement in Rod Bundle Subchannel by the Large Scale Secondary Vortex Flow," Ph. D. Thesis, The University of Korea. pp. 13~15, 64~66.

Rehme, K. and Trippe, G., 1980. "Pressure Drop And Velocity Distribution In Rod Bundle With Spacer Grids," *Nucl. Engng. And Design 62*, 349~359.

Shen, Y. F., Cao, Z. D. and Lu, Q. G., 1991, "An Investi-gation of Lateral Flow Mixing Effect Caused by Grid Spacer with Mixing Blades in a Rod Bundle," *Nucl. Engng. and Design 125*, pp. 111~119.

Wang, K. I., Dong, S. O. and Tae, H. C., 2001, "Flow Analysis for Optimum Design of Mixing Vane in a PWR Fuel Assembly," *Journal of the Korean Nuclear Society 33*, 27~338.

Yang, S. K. and Chung, M. K., 1996, "Measurements of Turbulent Flow in a 6 by 6 Rod Bundle with Spacer Grids," *J. of the Korean Nuclear Society 28*, 162~174.

Yang, S. K. and Chung, M. K., 1996. "Spacer Grid Effects on Turbulent Flow in Rod Bundles," *J. of the Korean Nuclear Society 28*, 56~71.

Yue, F. S., Zi, D. C. and Qing, G. L., 1991, "An Investigation of Crossflow Mixing Effect Caused by Grid Spacer with Mixing Blades in a Rod Bundle," *Nuclear Engineering and Design 125*, 111~119.